Electronic Supplementary Information

Defect-engineered WS_xSe_{2-x} nanocrystals anchored on the selenized polyacrylonitrile fibers toward high-performance sodium/potassium-ion batteries with wide temperature workability

Fuyu Xiao[a+], Jingran Zhang[a+], Weiming Zhou*[a], Yixing Fang*[a], Xiaotong He[a], Wenbin Lai[a], Chuyuan Lin[a], Mingyang Ge[a], Haosen Fan*[b], Qingrong Qian[a, c], Mingdeng Wei[d], Qinghua Chen[a, c] and Lingxing Zeng*[a, c]

[a] *Engineering Research Center of Polymer Green Recycling of Ministry of Education, Fujian Key Laboratory of Pollution Control & Resource Reuse, College of Environment and Resources, Fujian Normal University, Fuzhou, Fujian 350007, China. Email: zhouweiming721@126.com; fyx1993ustb@163.com; zenglingxing@fjnu.edu.cn*

[b] *College of Materials Science and Metallurgy Engineering, Guizhou University, Guiyang 550025, China. Email: hsfan@gzhu.edu.cn*

[c] *Key Laboratory of Advanced Energy Materials Chemistry (Ministry of Education), College of Chemistry, Nankai University, Tianjin 300071, China.*

[d] *Fujian Provincial Key Laboratory of Electrochemical Energy Storage Materials, Fuzhou University, Fuzhou, Fujian 350002, China.*

+ These authors contributed equally to this work.

Experimental Section

Synthesis of the WS_xSe_{2-x}-Se@PAN

Typically, polyacrylonitrile (PAN, 0.9 g, Mw=150 000, Sigma-Aldrich) and ammonium tetrathiotungstate ($(NH_4)_2WS_4$, 0.6 g, Sigma-Aldrich) were dissolved in 10 mL of N, Ndimethylformamide (DMF, 10 mL, A.R, Sinopharm Group Chemical Reagent Co., Ltd.) under stirring for 48 h at room temperature to a homogeneous solution. The solution was electrospun at 20 kV with a temperature of 40 ^oC. Then, the as-obtained electrospun fibres and selenium powder (A.R, Sinopharm Group Chemical Reagent Co. Ltd.) (w/w=1:1.5) were immersed and sonicated into carbon disulfide solution for 1 h. Finally, the precursor was calcined at 350℃ under 5% H_2/95% Ar atmosphere for 5 h at a ramp rate of 2 ^oC min^{-1} and then was continued to rise to 450 ^oC and maintained for 5h to acquire the WS_xSe_{2-x}-Se@PAN composite (denoted as WSSe -Se@PAN-2). For comparison, the WSSe -Se@PAN-1 and WSSe -Se@PAN-3 samples were synthesized *via* the same procedure by mixing the as-obtained electrospun fibers and selenium powder in different proportions with 1:1 and 1:2, respectively.

Material characterization

The scanning electron microscope (SEM, Hitachi 4800) and transmission electron microscope (TEM, FEI F20 S-TWIN) were used to study the microstructures of electrode materials. X-ray diffraction (XRD) patterns were collected on a Bruker D8 diffractometer (Germany) using a Cu Kα source in the range of 5-70°. FTIR spectroscopy and Raman spectra were examined on a DXR2xi (a diode laser of

excitation of 532 nm) and Thermo Scientific Nicolet iS10, respectively. Room temperature Electron paramagnetic resonance (EPR) spectra were collected on a MS 5000 spectrometer. The chemical states of the samples were recorded by X-ray photoelectron spectrometer (XPS) on a an ESCALAB MARK II spherical analyzer.

Electrochemical measurements

The electrochemical performance of Na/K-ion storage of all the electrodes were investigated by CR2032-type coin cells, which used pure sodium/potassium metal sheet as the counter/reference electrodes, the glass fiber film (Whatman GF/D) as separator. For the preparation of electrodes, active materials, super P and carboxymethyl cellulose binder (8:1:1 by weight) were milled together in deionized water to form uniform slurry. Then, the slurry was painted on a copper foil and dried at 80 ^{o}C in a vacuum for 12 h to obtain the working electrodes. The mass loading of the active material on each copper foil was typically about 1.0-1.5 mg cm^{-2}. 1.0 M $NaPF_6$ in EC/DMC/EMC (1:1:1, vol) with 5% FEC and 7.0 M KFSI in 100% DME were used as the electrolytes, respectively, for SIBs and PIBs. Furthermore, Sodium-ion full cell was assembled with $Na_3V_2(PO4)_3$ as cathode and as anode, Full cell assembly is similar to half-cell assembly, the WSSe -Se@PAN-2 (anode) and $Na_3V_2(PO_4)_3$ (cathode) is in the weight ratio of 1: 1.2, where the WSSe-Se@PAN-2 anode was presodiated for several cycles until the CE reached up to 95% before assembling full cells. Then they were coupled to fabricate the SIBs full cell in glove box. A LAND CT 2001A battery tester system was employed for investigating the galvanostatic charge/discharge performance, rate capabilities, and cycle performance with a voltage range of 0.01-3 V. Before the half-

cell wide temperature range performance test, the battery was pre-cycled 5 times at room temperature. A Ivium-n-Stat electrochemical workstation was used for testing the electrochemical impedance spectroscopy (EIS) (at a voltage amplitude 1.0 mV, and the frequency ranges from 10^{-1} Hz to 10^{5} Hz).

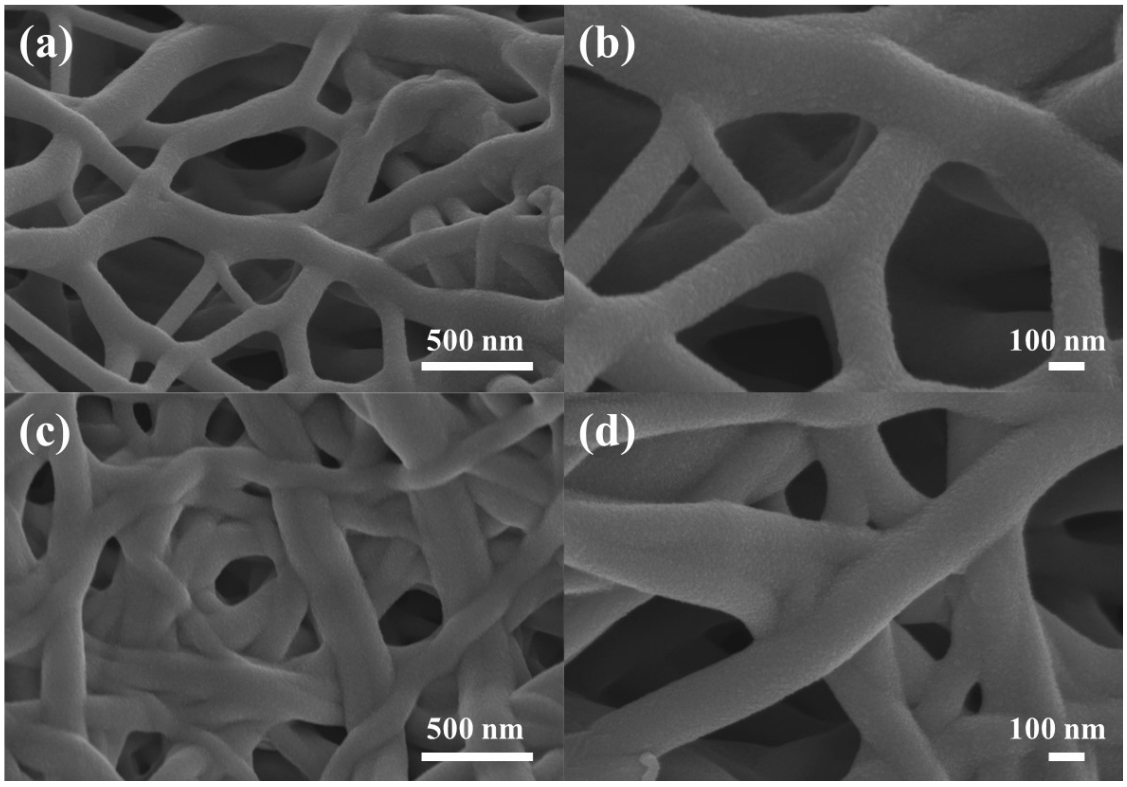

Figure S1 SEM images of (a and b) WSSe-Se@PAN-1 and (c and d) WSSe-Se@PAN-3.

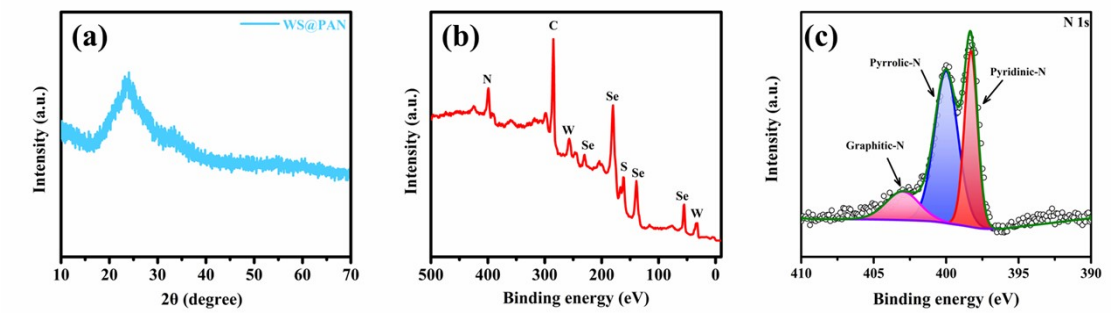

Figure S2 (a) XRD pattern of WS@PAN; XPS spectra of WSSe-Se@PAN-2: (b) survey spectrum and (c) N 1s.

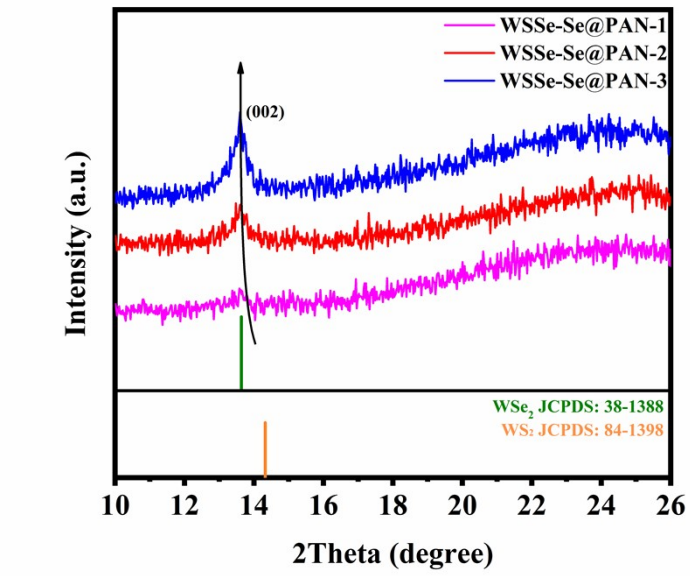

Figure S3 The XRD patterns of WSSe-Se@PAN-1, WSSe-Se@PAN-2 and WSSe-Se@PAN-3 between 10° and 26°.

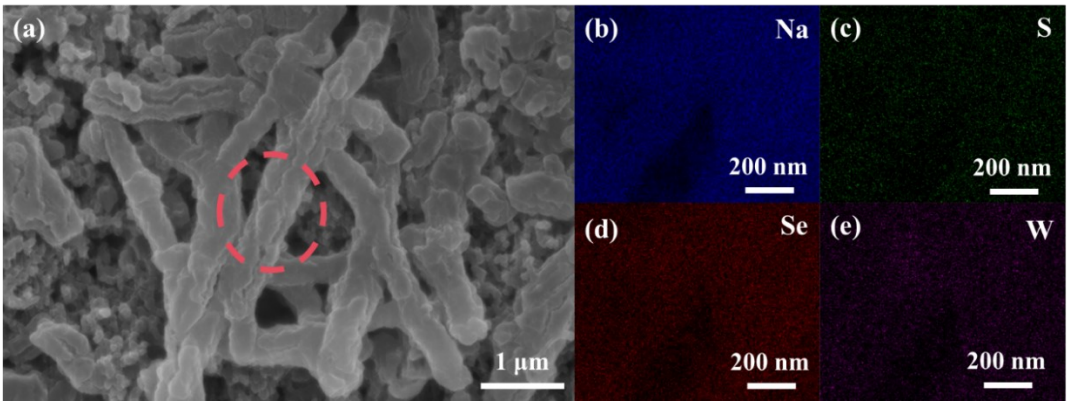

Figure S4 (a) The SEM image and (b) elemental mapping results of WSSe-Se@PAN-2 after 200 cycles test at 2 A g^{-1} for Na (blue), S (green), Se (red), W (purple).

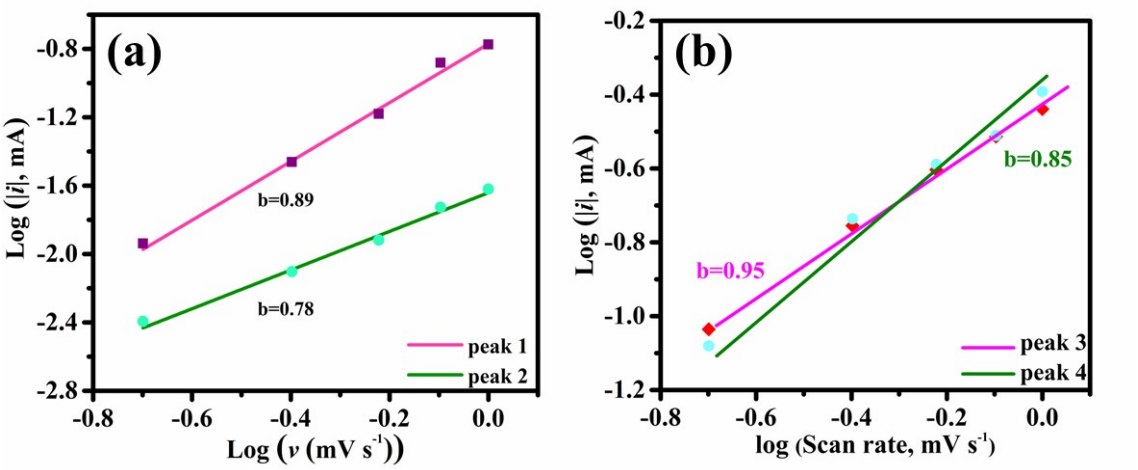

Figure S5 Log(i) versus log(v) plots at different oxidation and reduction peaks for (a) sodium ion batteries and (b) potassium-ion batteries, respectively.

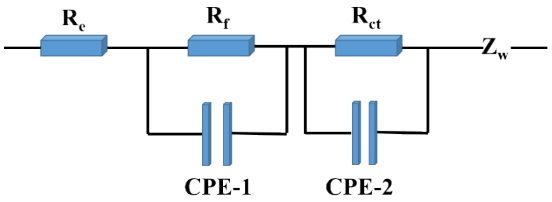

Fig. S6 the equivalent circuit for describing the EIS behavior of the studied system.

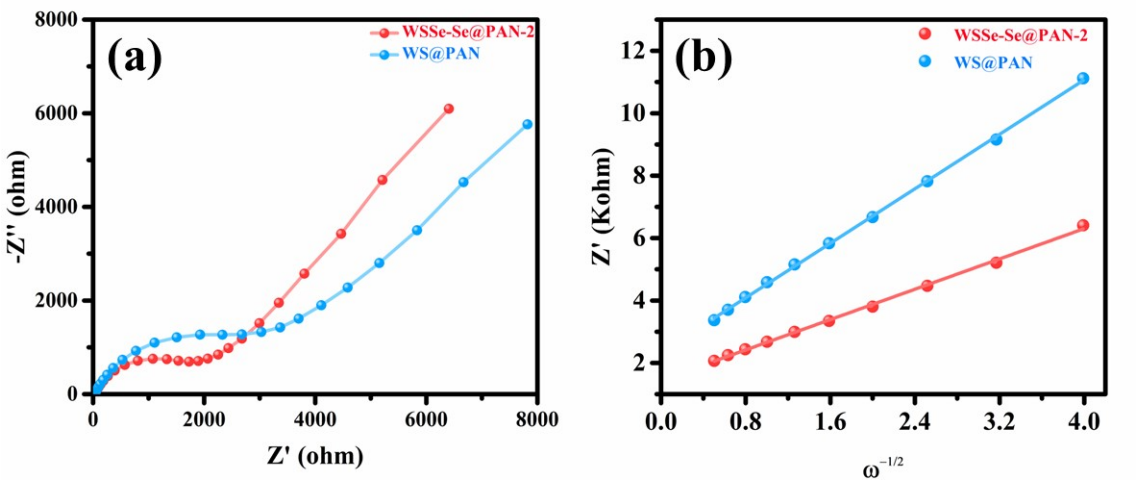

Figure S7 (a) EIS plots and (b) the relationship between Zre and $\omega^{-1/2}$ for WSSe-Se@PAN-2, and WS@PAN electrodes for potassium-ion batteries, respectively.

Table S1 Impedance parameters calculated from an equivalent circuit model.

sample	R_e (Ω)	R_f (Ω)	R_{ct} (Ω)	R_{total} (Ω)
WSSe-Se@PAN-1	**6.3**	**143.1**	**315.0**	**464.4**
WSSe-Se@PAN-2	**5.4**	**24.8**	**234.6**	**264.8**
WSSe-Se@PAN-3	**6.4**	**99.0**	**382.1**	**487.5**
WS@PAN	**6.7**	**141.3**	**546.7**	**694.7**

Table S2 The electrochemical rate performance of the related works of tungsten-based chalcogenides electrodes for sodium-ion batteries.

Electrode materials	Current density (A g^{-1})	Rate capability (mA h g^{-1})	Ref.
WS_2/NC	2.0	238.1	**[S1]**
WS_2 nanosheets	5.0	211.4	**[S2]**
H-WS_2@NC	8.0	254	**[S3]**
DODA-WS_2 nanofibers	10	91	**[S4]**
metallic WS_2 hollow microspheres	1.0	307.7	**[S5]**
WS_2@S/N–C	30	192	**[S6]**
PVD-deposited vertical WS_2/C	2.0	70	**[S7]**
WS_2@NC	5.0	151	**[S8]**
VA/LT-WS_2/C	5.0	103.8	**[S9]**
NB FeS_2/WS_2-CNFs	8.0	251.5	**[S10]**
WS_{2-x}/ZnS@C	20	181.9	**[S11]**
PCS/WS_2/NG	2.0	205.6	**[S12]**
H-WS_2	5.0	236.7	**[S13]**
1T $W_{0.9}Mo_{0.1}S_2$ nanoplates	5.0	245	**[S14]**
HB WS_2@CNFs	8.0	182.4	**[S15]**
WS_2–SPAN	10	270	**[S16]**
Ni-WS_2/GO	20	127	**[S17]**
WS_XSe_{2-X}-Se@PAN	**10**	**304**	**This work**

Table S3 Comparison of the electrochemical performance of the related literatures with wide-temperature workability.

Electrode Materials	**Field**	**Temperature (°C)**	**Current density (A g^{-1})**	**Cycling capability (mAh g^{-1})**	**Cycles**	**Ref.**
NbSSe	SIBs	0	0.03	136	500	[S18]
F-$CuFeS_2$@RGO	SIBs	-20	1	375	200	[S19]
		-40	1	182	200	
$FeS_{0.5}Se_{0.5}$@NC	SIBs	0	1	380.1	200	[S20]
$SnSe_2$-SePAN	SIBs	-15	0.5	300	700	[S21]
		60	0.5	352	100	
Bi	SIBs	-20	0.4	295	300	[S22]
		60	0.4	293.6	100	
WS_xSe_{2-x}-Se@PAN	**SIBs**	**50**	**1**	**313**	**1000**	**This work**
		-15	**1**	**76**	**1000**	

Table S4 The electrochemical performance of the related works of tungsten-based chalcogenides electrodes for potassium-ion batteries.

Electrode materials	**Current density (A g^{-1})**	**Cycling capability (mA h g^{-1})**	**Cycles**	**Ref.**
V_S-WS_2-SeNS	0.1	329	50	**[S23]**
C-WS_2@CNFs	0.1	312	100	**[S24]**
Commercial WS_2 powders	0.1	103	100	**[S25]**
S_v-WS_2	0.1	231	50	**[S26]**
WSe_2@N-doped C	0.1	302	120	**[S27]**
WSNC	0.1	384	200	**[S28]**
1T-WSe_2-Sn	0.1	345	50	**[S29]**
SP-K_xWSe_2	0.1	383	1000	**[S30]**
WS_xSe_{2-x}-Se@PAN	**0.1**	**466**	**100**	**This work**

References

S1 Y. Liu, H. Wei, C. Wang, F. Wang, H. Wang, W. Zhang, X. Wang, C. Yan, B. H. Kim and F. Ren, Nitrogen-doped carbon coated WS_2 nanosheets as anode for high-performance sodium-ion batteries, *Front. Chem.*, 2018, **6**, 236-244.

S2 Y. Wang, D. Kong, S. Huang, Y. Shi, M. Ding, Y. Von Lim, T. Xu, F. Chen, X. Li and H. Y. Yang, 3D carbon foam-supported WS_2 nanosheets for cable-shaped flexible sodium ion batteries, *J. Mater. Chem. A*, 2018, **6**, 10813-10824.

S3 X. Hu, Y. Liu, J. Li, G. Wang, J. Chen, G. Zhong, H. Zhan and Z. Wen, Self-assembling of conductive interlayer-expanded WS_2 nanosheets into 3d hollow hierarchical microflower bud hybrids for fast and stable sodium storage, *Adv. Funct. Mater.*, 2019, **30**, 1907677-1907689.

S4 X. Xu, X. Li, J. Zhang, K. Qiao, D. Han, S. Wei, W. Xing and Z. Yan, Surfactant assisted electrospinning of WS_2 nanofibers and its promising performance as anode material of sodium-ion batteries, *Electrochim. Acta*, 2019, **302**, 259-269.

S5 J. Wang, L. Yu, Z. Zhou, L. Zeng and M. Wei, Template-free synthesis of metallic WS_2 hollow microspheres as an anode for the sodium-ion battery, *J. Colloid Interf. Sci.*, 2019, **557**, 722-728.

S6 X. Li, Y. Sun, X. Xu, Y.-X. Wang, S.-L. Chou, A. Cao, L. Chen and S.-X. Dou, Lotus rhizome-like S/N–C with embedded WS_2 for superior sodium storage, *J. Mater. Chem. A*, 2019, **7**, 25932-25943.

S7 P. Li, Y. Wang, J. Y. Jeong, X. Gao, K. Zhang, A. Neville, S. Xu and J. H. Park, Vertically constructed monolithic electrodes for sodium ion batteries: toward low tortuosity and high energy density, *J. Mater. Chem. A*, 2019, **7**, 25985-25992.

S8 Y. V. Lim, Y. Wang, D. Kong, L. Guo, J. I. Wong, L. K. Ang and H. Y. Yang, Cubic-shaped WS_2 nanopetals on a prussian blue derived nitrogen-doped carbon nanoporous framework for high performance sodium-ion batteries, *J. Mater. Chem. A*, 2017, **5**, 10406-10415.

S9 S. Xu, X. Gao, Y. Hua, A. Neville, Y. Wang and K. Zhang, Rapid deposition of WS_2 platelet thin films as additive-free anode for sodium ion batteries with superior volumetric capacity, *Energy Storage Mater.*, 2020, **26**, 534-542.

S10 H. Wu, N. Xu, Z. Jiang, A. Zheng, Q. Shi, R. Lv, L. Ni, G. Diao and M. Chen, Space and interface confinement effect of necklace-box structural FeS_2/WS_2 carbon nanofibers to enhance Na^+ storage performance and electrochemical kinetics, *Chem. Eng. J.*, 2022, **427**, 131002-131012.

S11 Y. Li, J. Qian, M. Zhang, S. Wang, Z. Wang, M. Li, Y. Bai, Q. An, H. Xu, F. Wu, L. Mai and C. Wu, Co-construction of sulfur vacancies and heterojunctions in tungsten disulfide to induce fast electronic/ionic diffusion kinetics for sodium-ion batteries, *Adv. Mater.*, 2020, **32**, e2005802.

S12 T. Li, R. Guo, Y. Luo, F. Li, L. Meng, X. Sun, Z. Yang, H. Luo and Y. Wan, Improved lithium and sodium ion storage properties of WS_2 anode with three-layer shell structure, *Electrochim. Acta*, 2020, **331**, 135424-135437.

S13 X. Luo, J. Huang, Y. Huang, L. Cao, J. Li, Y. Wang, Z. Xu, S. Wei and K. Kajiyoshi, Self-templated induced carbon-supported hollow WS_2 composite structure for high-performance sodium storage, *J. Mater. Chem. A*, 2021, **9**, 21366-21378.

S14 H. Tao, J. Li, J. Li, Z. Hou, X. Yang and L.-Z. Fan, Metallic phase $W_{0.9}Mo_{0.1}S_2$ for high-performance anode of sodium ion batteries through suppressing the

dissolution of polysulfides, *J. Energy Chem.*, 2022, **66**, 356-365.
S15 H. Wu, X. Chen, C. Qian, H. Yan, C. Yan, N. Xu, Y. Piao, G. Diao and M. Chen, Confinement growth of layered WS_2 in hollow beaded carbon nanofibers with synergistic anchoring effect to reinforce Li^+/Na^+ storage performance, *Small*, 2020, **16**, e2000695.
S16 Z. Lei, J. Zheng, X. He, Y. Wang, X. Yang, F. Xiao, H. Xue, P. Xiong, M. Wei, Q. Chen, Q. Qian and L. Zeng, Defect-rich WS_2–SPAN nanofibers for sodium/potassium-ion batteries: ultralong lifespans and wide-temperature workability, *Inorg. Chem. Front.*, 2023, **10**, 1187-1196.
S17 X. Luo, J. Huang, L. Cao, J. Li, Z. Xu, K. Kajiyoshi, Y. Zhao, H. Yang, Y. Liu and Z. Li, Constructing multi-dimensional migration channel by nickel-doped WS_2 composite: High speed sodium and potassium ion storage kinetics in WS_2 nanosheets, *Chem. Eng. J.*, 2023, **464**, 142579-142590.
S18 Zhou, L.-F.; Gao, X.-W.; Du, T.; Gong, H.; Liu, L.-Y.; Luo, W.-B. Two-dimensional NbSSe as anode material for low-temperature sodium-ion batteries. *Chem. Eng. J.,* 2022, **435,** 134838-134844.
S19 G. Sun, H. Lin, R. Tian, Z. Wei, X. Wang, X. Jin, S. Yao, G. Chen, Z. Shen and F. Du, Rational design and synthesis of nanosheets self-assembled hierarchical flower-ball-like $CuFeS_2$ for boosted wide temperature sodium-ion batteries, *Nano Res.*, 2023, **16**, 9407-9415.
S20 Y. Wang, Y. Liu, Q. Li, Z. Li, A. Xu, C. Dong, J. Sun, X. Zhang, X. Sun, J. Yang, F. Jiang and Y. Zhou, New dual-anions $FeS_{0.5}Se_{0.5}$@NC porous nanorods as advanced electrode materials for wide-temperature sodium-ion half/full batteries, *Appl. Surf. Sci.*, 2023, **620,** 156836-156845.
S21 Y. Wang, F. Xiao, X. Chen, P. Xiong, C. Lin, H. Wang, M. Wei, Q. Qian, Q Chen, L. Zeng, Extraordinarily stable and wide temperature range sodium/potassium-ion batteries based on 1D $SnSe_2$-SePAN composite nanofibers, *InfoMat*, 2023, **5**, 12467.
S22 J. Zhou, Y. Ding, Y. Wang, H. Li, J. Shang, Y. Cao and H. Wang, Bulk bismuth anodes for wide-temperature sodium-ion batteries enabled by electrolyte chemistry modulation, *J. Colloid Interf. Sci.*, 2024, **657**, 502-510.
S23 Q. Zhu, W. Li, J. Wu, N. Tian, Y. Li, J. Yang and B. Liu, Filling selenium into sulfur vacancies in ultrathin tungsten sulfide nanosheets for superior potassium storage, *ACS Appl. Mater. interfaces*, 2022, **14**, 51994-52006.
S24 S. Geng, T. Zhou, M. Jia, X. Shen, P. Gao, S. Tian, P. Zhou, B. Liu, J. Zhou, S. Zhuo and F. Li, Carbon-coated WS_2 nanosheets supported on carbon nanofibers for high-rate potassium-ion capacitors, *Energy Environ. Sci.*, 2021, **14**, 3184-3193.
S25 Y. Wu, Y. Xu, Y. Li, P. Lyu, J. Wen, C. Zhang, M. Zhou, Y. Fang, H. Zhao, U. Kaiser and Y. Lei, Unexpected intercalation-dominated potassium storage in WS_2 as a potassium-ion battery anode, *Nano Res.*, 2019, **12**, 2997-3002.
S26 Q. Zhu, W. Li, J. Wu, N. Tian, Y. Li, J. Yang, B. Liu and J. Jiang, Vacancy engineering in WS_2 nanosheets for enhanced potassium‐ion storage, *J. Power Sources*, 2022, **542**, 231791-231801.
S27 X. Chen, H. Muheiyati, X. Sun, P. Zhou, P. Wang, X. Ding, Y. Qian and L. Xu, Rational design of tungsten selenide@N-doped carbon nanotube for high-stable potassium-ion batteries, *Small*, 2022, **18**, e2104363.
S28 L. Xing, K. Han, Q. Liu, Z. Liu, J. Chu, L. Zhang, X. Ma, Y. Bao, P. Li and W. Wang, Hierarchical two-atom-layered WSe_2/C ultrathin crumpled nanosheets

assemblies: Engineering the interlayer spacing boosts potassium-ion storage, *Energy Storage Mater.*, 2021, **36**, 309-317.

S29 Y.-R. Liu, Z.-W. Lei, R.-P. Liu, X.-Y. Li, P.-X. Xiong, Y.-J. Luo, Q.-H. Chen, M.-D. Wei, L.-X. Zeng and Q.-R. Qian, Sn-doped induced stable 1T-WSe_2 nanosheets entrenched on N-doped carbon with extraordinary half/full sodium/potassium storage performance, *Rare Met*., 2023 **42**, 1557-1569

S30 Z. Zhao, T. Xu and X. Yu, Unlock the potassium storage behavior of singlephased tungsten selenide nanorods via large cation insertion, *Adv. Mater.*, 2022, **35**, 2208096-2208106.